Impacts of wind stress on the Antarctic Circumpolar Current fronts and associated subduction

S. M. Downes,[1] A. S. Budnick,[1] J. L. Sarmiento,[1] and R. Farneti[2]

Received 4 April 2011; revised 7 May 2011; accepted 9 May 2011; published 14 June 2011.

[1] Recent studies suggest that the overturning circulation in the Antarctic Circumpolar Current (ACC) region shows a weak sensitivity to overlying wind stress changes, due to balancing of changes in the eddy-induced and Eulerian mean transports. Using an eddy-permitting coupled climate model, we analyze the response of the ACC transport, and associated water mass subduction rates, in response to an idealized poleward shift and intensification of the westerlies. As in previous studies, we find a small increase in the net ACC transport, and a poleward shift in the mean position of the ACC flow. However, the ACC is restructured, with the Subantarctic Front (SAF) and Polar Front (PF) branches shifting poleward by between 0.9° and 2.5° of latitude, resulting in a weaker ACC flow in both the SAF and PF zones. The wind stress anomaly drives a stronger northward Ekman transport of cool surface waters, deepening the winter mixed layer and causing a 12.7 Sv increase in the subduction of Subantarctic Mode Water (SAMW) north of the SAF zone and a 6.5 Sv increase in the subduction of Antarctic Intermediate Water (AAIW) within the SAF and PF zones. Our results suggest that changes in the wind stress restructure the Southern Ocean large-scale circulation, including the flow of the ACC in its primary jets, and that this affects the formation rates of SAMW and AAIW in this complex region. **Citation:** Downes, S. M., A. S. Budnick, J. L. Sarmiento, and R. Farneti (2011), Impacts of wind stress on the Antarctic Circumpolar Current fronts and associated subduction, *Geophys. Res. Lett.*, *38*, L11605, doi:10.1029/2011GL047668.

1. Introduction

[2] The Southern Ocean and the Antarctic Circumpolar Current (ACC) are a focal point for water mass formation, biological productivity, and the uptake and transport of heat and dissolved gases between basins. The strength of the ACC and the position of its associated fronts is influenced by the overlying westerly wind stress, friction, bottom drag and topography [*Gnanadesikan and Hallberg*, 2000; *Rintoul et al.*, 2001]. Recent observationally-based estimates [*Böning et al.*, 2008] and fine resolution model studies [*Hallberg and Gnanadesikan*, 2006; *Farneti et al.*, 2010; *Farneti and Delworth*, 2010] indicate that an increase in the strength of the overlying westerlies has an overall minimal impact on the transport and isopycnal tilt of the ACC. However, the degree to which the associated eddy-induced overturning circulation compensates for changes in the Eulerian mean flow remains under debate. *Farneti et al.* [2010] show a partial eddy compensation to changing wind regimes, implying possible changes in water mass subduction. Based on the eddy-permitting model of *Farneti et al.* [2010], we show that a minimal change in the ACC strength under an increased westerlies scenario does not necessarily preclude restructuring of the large-scale flow and transport in the ACC region. We focus here on the ocean response in the Subantarctic Front (SAF) and Polar Front (PF) zones, within which most of the ACC transport is carried [*Rintoul and Sokolov*, 2001].

[3] Two Southern Ocean water masses, Subantarctic Mode Water (SAMW) and Antarctic intermediate Water (AAIW), form within and north of the SAF and PF zones, partially as a result of upwelled deep waters driven equatorward across the ACC. SAMW and AAIW ventilate the Southern Hemisphere subtropical gyres via the process of subduction, and are associated with large anthropogenic CO_2 uptake [*Sabine et al.*, 2004], as well as nutrient supply to the main thermocline [*Sarmiento et al.*, 2004]. In a global warming scenario, many coarse-resolution models project a decrease in the subduction of SAMW and AAIW due to increased surface warming and freshening [*Downes et al.*, 2010]. In this paper we show that, in the absence of global warming, strengthened westerlies may still significantly change the subduction rate of water masses in the ACC region, despite having little impact on the ACC density structure.

2. Model and Methods

[4] We employ an eddy-permitting coupled model, CM2.4, recently developed at the NOAA/ Geophysical Fluid Dynamics Laboratory. The ocean component is the Modular Ocean Model, version 4 [*Griffies et al.*, 2003] with a 1/4° horizontal resolution that increases poleward, and fifty depth levels in the vertical. There is no parameterization of eddy-induced transport and background diffusivity in the model. The atmospheric component is the 1° horizontal resolution model of *Delworth et al.* [2006]. We compare two 40 year periods from a control (CTL) and wind perturbation (SHW3X) experiment, as described by *Delworth and Zeng* [2008] and *Farneti et al.* [2010]. The 240-year long CTL run uses a present day 1990-radiative forcing. The model is not run to steady state. However, we have tested our results using different averaged periods, and have found them to be robust for the 40-year period chosen within the second century of output. In theSHW3X case we apply a wind stress anomaly between 75°S and 20°S, multiplied by a factor of three to emphasize the amplitude of the response of the ACC region [see *Farneti et al.*, 2010, Figure 4]. The fixed anomaly

[1]Program in Atmospheric and Oceanic Sciences, Princeton University, Princeton, New Jersey, USA.
[2]Earth System Physics Section, ICTP, Trieste, Italy.

0094-8276/11/2011GL047668

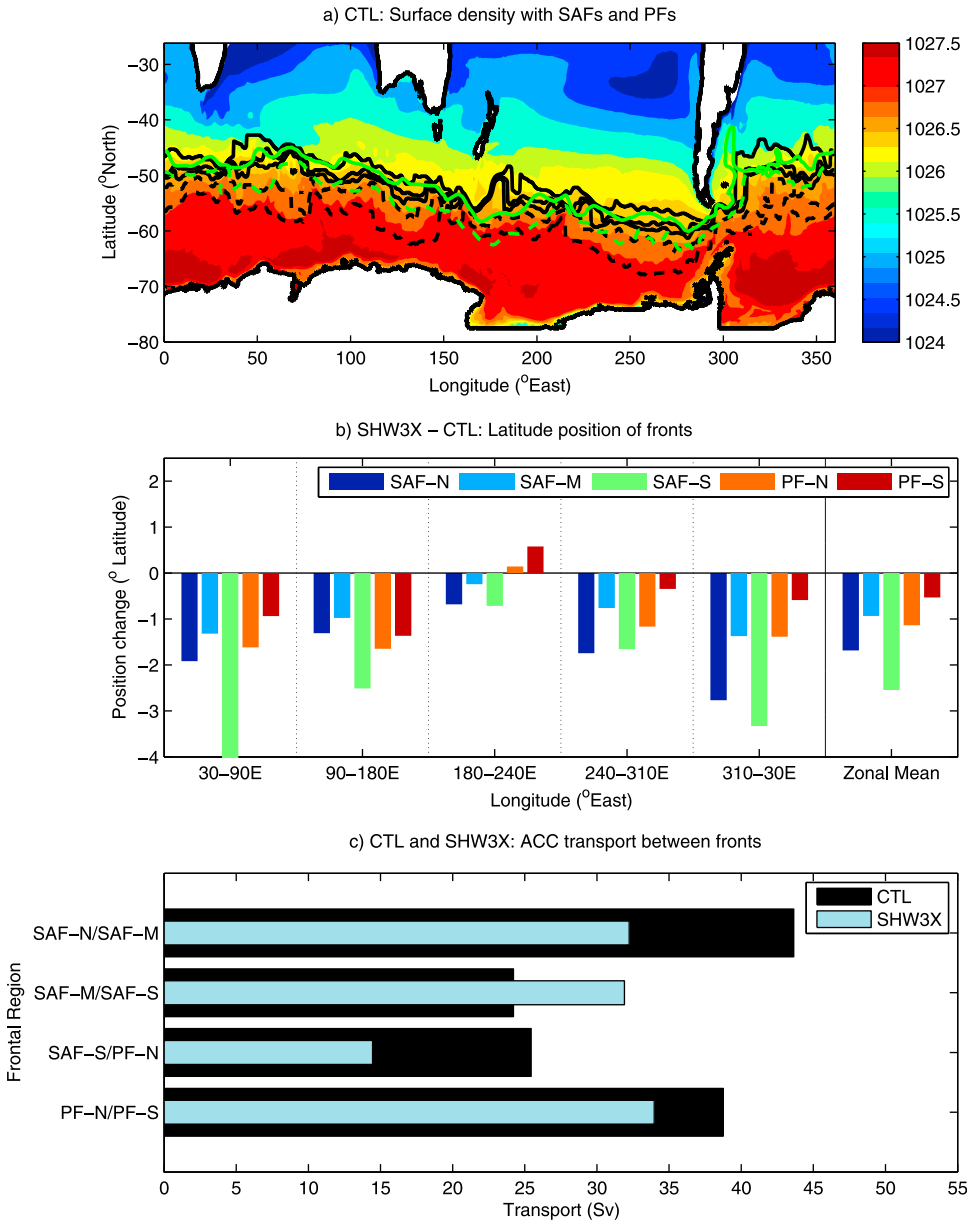

Figure 1. (a) Surface potential density (kg m^{-3}) overlaid with (from north to south): northern, middle and southern SAF branches (black solid), and the northern and southern PF branches (black dashed). The mean SAF and PF branches as defined hydrographically by *Orsi et al.* [1995] are overlaid in green. (b) Difference (SHW3X minus CTL) in the latitudinal position of the three SAF branches (SAF-N, SAF-M and SAF-S) and two PF branches (PF-N and PF-S); see legend for corresponding colors. The trends are averaged over zonal sections (given in longitude degrees East) and the zonal mean change is also shown. Negative change indicates a poleward shift in the front, and positive values indicate an equatorward shift.(c) ACC transport flowing between the Subantarctic and Polar Front branches for the CTL (black) and SHW3X (blue) experiments. Units are in Sv, where 1 Sv = 10^6 m^3 s^{-1}.

is based on the difference in wind stress in the coarse-resolution model CM2.1 [*Delworth et al.*, 2006] between the late twentieth and twenty-first centuries for the Intergovernmental Panel on Climate Change (IPCC) A1B scenario. *Farneti et al.* [2010] showed that adding in the anomaly causes a southward shift and strengthening of the westerlies south of 45°S.

[5] To determine the locations of the SAF and PF branches in the ACC region, we used the sea-surface height method of *Sokolov and Rintoul* [2002, 2007] applied to each monthly snapshot of the 40-year time series. The fronts are defined by the sea surface height (SSH) contours that correspond to maxima in the meridional SSH gradient. While *Sokolov and Rintoul* [2007] found 10 ACC fronts using a minimizing area function around the frontal jets, the CM2.4 ocean model resolution permitted detection of six fronts. We associated five of these fronts with the SAF and PF branches by comparison with hydrographic temperature and depth definitions of the fronts from *Orsi et al.* [1995] (Figure 1a). The sixth front was located within the subtropical region and is not associated with the flow of the ACC. Fronts south of the southern Polar Front branch were difficult to identify

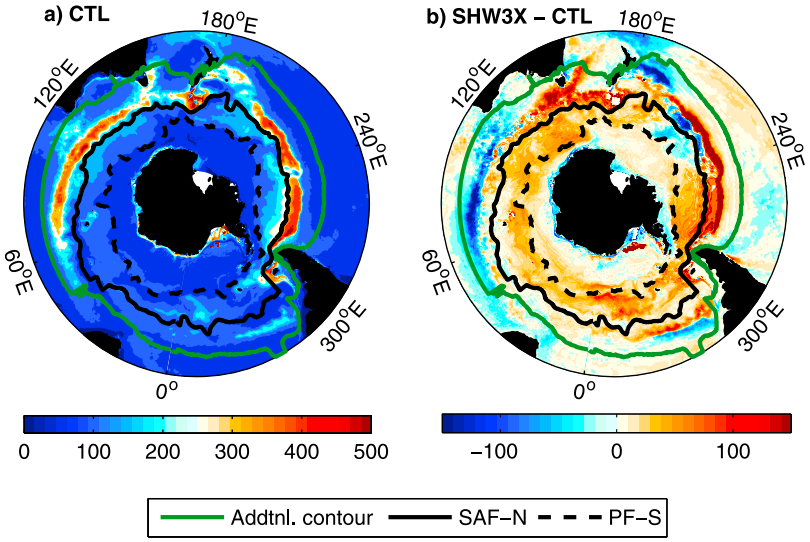

Figure 2. (a) CTL winter mixed layer depth (m) defined by a 0.03 kg m^{-3} density criteria. Overlaid are the SAF-N (black solid) and PF-S (black dashed) branches. The green curve represents the additional contour defined as 0.8 kg m^{-3} less than the density of the SAF-N branch. (b) Difference (SHW3X minus CTL) in the winter mixed layer depth (m), overlaid with the same two fronts and green additional contour as in Figure 2a.

because of weak SSH gradient directly north of the Antarctic continent.

3. Results

3.1. ACC Fronts and Transport

[6] In the CTL run, the three SAF branches (SAF-N, SAF-M and SAF-S) agree well with the observed location of the mean SAF position of *Orsi et al.* [1995], who define fronts according to hydrographic data (Figure 1a). However the observed mean PF branch corresponds more with the model northern PF branch (PF-N) than the southern PF branch (PF-S), possibly due to the discrepancies in the observed PF temperature criteria in some parts of the Southern Ocean [see *Sokolov and Rintoul*, 2007, Figure 7]. We find that the wind stress changes shift the position of the SAF and PF branches poleward by a zonal mean of between 0.9° and 2.5° latitude (Figure 1b). The SAF-S branch is shifted by the greatest amount in the Indian and Atlantic basins, and the SAF-N is shifted the most in the Pacific basin.

[7] One of the consequences of the nonuniform poleward shift in the SAF and PF branches is a redistribution of the ACC mean flow. The ACC transport through Drake Passage in the CTL experiment is 189 Sv, 132 Sv of which is carried between the northern SAF and southern PF branches (Figure 1c). The CTL ACC transport is larger than the observed rate of ~135 Sv [e.g., *Cunningham et al.*, 2003], however model studies have shown that the response of the ACC transport for the SHW3X case, and under global warming scenarios with weaker wind stress anomalies, is not affected by the size of the present day ACC transport [*Farneti et al.*, 2010; *Sen Gupta et al.*, 2009]. In the SHW3X case, we find that the net ACC transport increases by 12 Sv, however, the frontal position changes lead to an increase of 7 Sv between the SAF-M and SAF-S branches, and a decrease in transport of 5 to 11 Sv between the other SAF and the PF branches. Combined, the ACC transport in the SAF and PF zones decreases by 19 Sv, as more of the ACC is carried south of the PF-S branch. This reorganization of the ACC flow due to wind stress changes directly impacts water mass subduction and inter-basin exchange of heat and nutrients.

3.2. Subduction of Southern Ocean Water Masses

[8] We calculate the net subduction rate (S_{ann}) using the definition of *Marshall et al.* [1993]: $S_{ann} = -\mathbf{u}_H \cdot \nabla H - w_H$. The lateral induction term, $\mathbf{u}_H \cdot \nabla H$, represents the horizontal velocities ($\mathbf{u}_H$) intersecting the slope of the maximum mixed layer depth in the annual cycle (i.e., the winter mixed layer depth; H). The second term, w_H, is the upward vertical velocity at the winter mixed layer base. We use a mixed layer depth density criterion of $|\rho_m - \rho_s| = 0.03$ kg m^{-3}, where ρ_m is the density at the base of the mixed layer and ρ_s is the surface density. We use the winter mixed layer for estimating S_{ann} to represent the exchange between the mixed layer and the main thermocline, and exclude transfer between the mixed layer and the seasonal thermocline. A positive S_{ann} indicates that the *subduction* of fluid *from* the mixed layer into the main thermocline during spring (as the winter mixed layer shoals) dominates the annual rate, and a negative S_{ann} indicates that *obduction* into the mixed layer from the ocean interior (as the mixed layer deepens in winter) is greater than the subduction. We integrate S_{ann} over the horizontal grid area to give units of Sv (where 1 Sv = 10^6 m^3 s^{-1}).

[9] The CTL winter mixed layer depth exceeds 400 m north of the SAF-N branch, in the southeast Indian and Pacific basins (Figure 2a), comparing well to recent observations [e.g., *Dong et al.*, 2008]. To later discuss the subduction in the deep winter mixed layer regions, we define an additional contour that is 0.8 kg m^{-3} less than the density at the SAF-N contour (green curve in Figure 2). In the SHW3X case, the winter mixed layer depth deepens by over 80 m, most significantly in the Pacific basin north of the SAF (Figure 2b), exhibiting a spatial pattern similar to that found for a positive Southern Annular Mode phase over

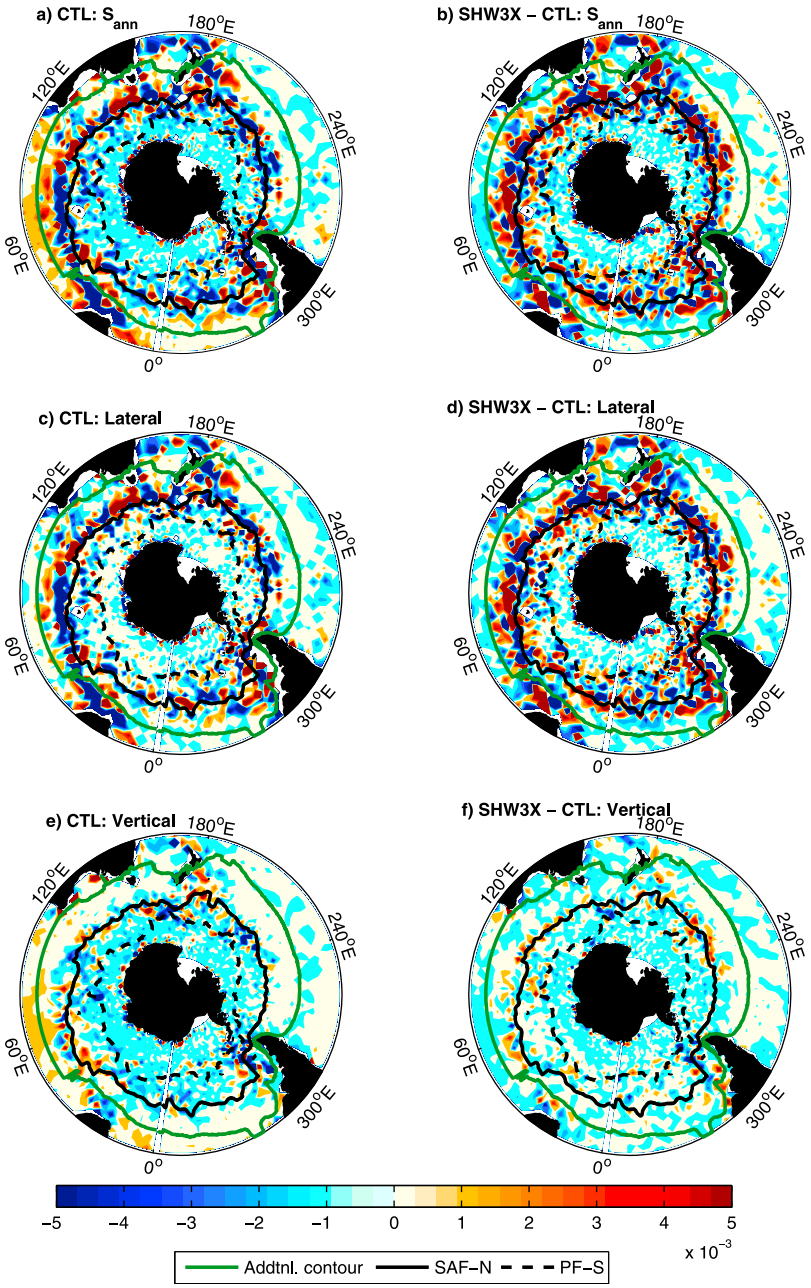

Figure 3. Annual mean subduction (S_{ann}; Sv) for (a) CTL and (b) SHW3X minus CTL. The overlaid fronts and additional contour are the same as in Figure 2. Positive S_{ann} indicates subduction into the main thermocline dominates the annual cycle, and negative indicates obduction into the mixed layer dominates. The subduction rate is divided into the (c and d) lateral and (e and f) vertical components.

the last decade of *Sallée et al.* [2010a]. *Sallée et al.* [2010a] concluded that changes in the air-sea heat flux (i.e., latent, sensible and radiative fluxes) were the dominant processes leading to the mixed layer changes. However, in this study where only the westerlies are perturbed, we find that the heat carried by the Ekman transport plays a dominant role. Increases in the Ekman transport of cool surface waters deepen the winter mixed layer in the eastern Pacific and within the SAF and PF zones. By contrast, the strong shoaling of the winter mixed layer in the east Indian region is due to a decrease in the heat loss from both the air-sea fluxes and Ekman heat fluxes.

[10] The CTL S_{ann} repeatedly changes sign and has multiple areas of strong subduction across the ACC region (Figure 3a), as observed in recent studies [e.g., *Karstensen and Quadfasel*, 2002; *Sallée et al.*, 2010b]. The large-scale regions of high subduction rates (i.e., positive S_{ann}), between the black solid SAF-N branch and green additional contour, occur in regions of deep mixed layers (Figure 2a), where the dominant subduction mechanism is lateral induction (Figure 3c). The vertical subduction term is essentially comprised of Ekman pumping and suction and the convergence of transport within the mixed layer. We find that obduction is prevalent within, and south of, the PF

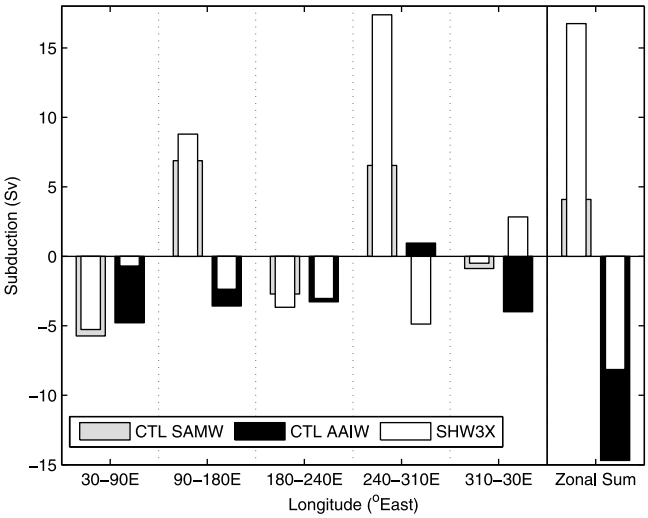

Figure 4. Annual mean subduction (S_{ann}; Sv) summed over five zonal sections and the total sum for SAMW (σ_0 = 1025.5–1026.5 kg m^{-3}) and AAIW (σ_0 = 1026.5–1027.0 kg m^{-3}). The CTL case is shown in grey bars for SAMW, and black bars for AAIW. The overlaid white bars represent the SAMW and AAIW S_{ann} in the SHW3X case. Positive values represent subduction dominating annual cycle; negative values indicate obduction dominates.

zone, where the vertical term dominates due to Ekman suction of deep waters into the mixed layer (Figure 3e).

[11] The response of S_{ann} in the SHW3X case (Figure 3b) is mostly dominated by the lateral subduction component (Figure 3d), particularly in regions where the mixed layer deepens strongly, such as north of the SAF zone in the Pacific basin, and less so in the SAF and PF zones (Figure 2b). However, in the Indian and Atlantic basins the decreases in subduction north of the SAF zone are controlled by decreases in both the lateral (where the winter mixed layer shoals) and vertical (Figure 3f) components. South of the PF zone, the negative S_{ann} increases, due to increases in Ekman suction in the vertical subduction term. These subduction rate changes imply that both uptake of anthropogenic carbon and outgassing of natural carbon would increase in response to increased westerlies.

[12] We define SAMW as having a potential density of between 1025.5 and 1026.5 kg m^{-3} (low potential vorticity layer) and we define AAIW as having a density of between 1026.5 and 1027.0 kg m^{-3} (salinity minimum layer), noting that the CM2.4 model has a lighter density structure than observed. We average S_{ann} over five large regions (Figure 4) to smooth over the variations in sign and magnitude across the circumpolar belt (see Figure 3). We find that a total of 4.1 Sv of SAMW (grey bars) subducts in the CTL case, dominated by high rates in the east Indian and Pacific basins where deep winter mixed layers are found. The annual net subduction rate for AAIW is negative (black bars; −14.7 Sv), indicating that obduction prevails in the seasonal cycle and that the net formation of AAIW occurs primarily within the permanent thermocline. The net subduction rate of SAMW and AAIW combined increases by 6.1 Sv in the SHW3X case, dominated by a tripling of the net SAMW subduction rate to 12.7 Sv, particularly due to increased subduction in the eastern Pacific. Overall, the negative S_{ann} for AAIW decreases by 6.6 Sv in the SHW3X case. The change in the subduction of SAMW varies regionally, because the winter mixed layer response is non-uniform around the circumpolar belt. However, the regional variations in both the winter mixed layer and the vertical subduction term control the regional response of AAIW subduction.

4. Concluding Remarks

[13] We have used an eddy-permitting coupled model to diagnose the response of the large-scale flow in the ACC region in response to an increase and shift in the overlying westerly wind stress. *Farneti et al.* [2010] compared the same SHW3X and CTL experiments and showed that the CM2.4 model is near an eddy-saturated state, as its ACC transport is nearly independent of wind stress forcing. However, both the Eulerian mean and eddy-induced overturning circulation significantly respond to the large SHW3X wind stress anomaly, as well as a comparatively smaller anomaly associated with the IPCC A1B scenario [see *Farneti et al.*, 2010, Figure 10]. Here we chose a very strong anomaly in order to discern and highlight the response of the Southern Ocean fronts and associated ventilation rates, as the ACC horizontal flow remains unchanged. This paper builds on the results of *Farneti et al.* [2010b] by showing that, despite a weak change in the net ACC strength, there is a redistribution of the ACC transport. We find that a large poleward shift of the SAF and PF branches results in little net change in ACC transport in the SAF zone, but shows a decrease in ACC flow in the PF zone, compensated by an increased ACC transport further south. *Sokolov and Rintoul* [2009] observed that the SAF and PF shifted about 60 km poleward between 1992 and 2007. Isolating the impact of winds, we find here a poleward shift of between 100 and 300 km over a 40year period. We note that the wind stress anomaly applied here far exceeds what was observed between 1992 and 2007. Therefore, any comparisons with observations, whether explicit or implicit, as is the case here, should be made cautiously.

[14] There are significant increases in subduction north of, and within, the SAF and PF zones where SAMW and AAIW subduct. These increases are dominated by the lateral induction term, as increased heat loss due to northward Ekman transport increases the winter mixed layer gradient. South of the PF zone, the stronger westerlies increase Ekman suction of deep waters. Our regionally dependent subduction changes in the ACC region would likely impact upwelling of nutrients and biological growth and grazing rates [e.g., *Abbott et al.*, 2001; *Hunt et al.*, 2002], and the storage of and outgassing of carbon. Our results suggest that studies focusing on the response of the ACC region to wind stress anomalies should assess the regional distribution of changes in the ACC frontal system and the water mass flow as an accompaniment to zonal averages and net changes.

[15] **Acknowledgments.** The authors wish to thank Anand Gnanadesikan, Eun Young Kwon, Thomas Frölicher, and two anonymous reviewers for constructive comments on the manuscript. We gratefully acknowledge GFDL scientists, in particular Fanrong Zeng and Thomas Delworth, for their modeling efforts. This research was supported by NOAA grant NA07OAR4310096.

[16] The Editor thanks two anonymous reviewers for their assistance in evaluating this paper.

References

Abbott, M. R., J. G. Richman, J. S. Nahorniak, and B. S. Barksdale (2001), Meanders in the Antarctic Polar Frontal Zone and their impact on phytoplankton, *Deep Sea Res., Part II*, *48*, 3891–3912.

Böning, C. W., A. Dispert, M. Visbeck, S. Rintoul, and F. U. Schwarzkopf (2008), Antarctic Circumpolar Current response to recent climate change, *Nat. Geosci.*, *1*, 864–869.

Cunningham, S. A., S. G. Alderson, B. A. King, and M. A. Brandon (2003), Transport and variability of the Antarctic Circumpolar Current in Drake Passage, *J. Geophys. Res.*, *108*(C5), 8084, doi:10.1029/2001JC001147.

Delworth, T. L., and F. Zeng (2008), Simulated impact of altered Southern Hemisphere winds on the Atlantic meridional overturning circulation, *Geophys. Res. Lett.*, *35*, L20708, doi:10.1029/2008GL035166.

Delworth, T. L., et al. (2006), GFDL CM2 global coupled climate models. Part I: Formulation and simulation characteristics, *J. Clim.*, *19*, 643–674.

Dong, S., J. Sprintall, S. T. Gille, and L. Talley (2008), Southern Ocean mixed-layer depth from Argo float profiles, *J. Geophys. Res.*, *113*, C06013, doi:10.1029/2006JC004051.

Downes, S. M., N. L. Bindoff, and S. R. Rintoul (2010), Changes in the subduction of Southern Ocean water masses at the end of the 21st century in eight IPCC models, *J. Clim*, *23*, 6526–6541, doi:10.1175/2010JCLI3620.1.

Farneti, R., and T. L. Delworth (2010), The role of mesoscale eddies in the remote oceanic response to altered Southern Hemisphere winds, *J. Phys. Oceanogr.*, *40*, 2348–2354.

Farneti, R., T. L. Delworth, A. J. Rosati, S. M. Griffies, and F. Zang (2010), The role of mesoscale eddies in the rectification of the Southern Ocean response to climate change, *J. Phys. Oceanogr.*, *40*, 1539–1557.

Gnanadesikan, A., and R. W. Hallberg (2000), On the relationship of the circumpolar current to Southern Hemisphere winds in coarse-resolution ocean models, *J. Phys. Oceanogr.*, *30*, 2013–2034.

Griffies, S. M., M. J. Harrison, R. C. Pacanowski, and A. Rosati (2003), A technical guide to MOM4, *Tech. Rep. 5*, 295 pp., Geophys. Fluid Dyn. Lab., Princeton, N. J.

Hallberg, R. W., and A. Gnanadesikan (2006), The role of eddies in determining the structure and response of the wind-driven Southern Hemisphere overturning: Results from the modeling eddies in the Southern Ocean (MESO) project, *J. Phys. Oceanogr.*, *36*, 2232–2252.

Hanawa, K., and L. D. Talley (2001), Mode Waters, in *Ocean Circulation and Climate*, edited by G. Siedler, J. Church, and J. Gould, pp. 373–386, Academic, San Diego, Calif.

Hunt, B. P. V., E. A. Pakhomov, and C. D. McQuaid (2002), Community structure of mesozooplankton in the Antarctic polar frontal zone in the vicinity of the Prince Edward Islands (Southern Ocean): Small-scale distribution patterns in relation to physical parameters, *Deep Sea Res., Part II*, *49*, 3307–3325.

Karstensen, J., and D. Quadfasel (2002), Formation of Southern Hemisphere thermocline waters: Water mass conversion and subduction, *J. Phys. Oceanogr.*, *32*, 3020–3038.

Marshall, J. C., A. J. G. Nurser, and R. G. Williams (1993), Inferring the subduction rate and period over the North Atlantic, *J. Phys. Oceanogr.*, *23*, 1315–1329.

Orsi, A. H., T. Whitworth III, and W. D. Nowlin Jr. (1995), On the meridional extent and fronts of the Antarctic Circumpolar Current, *Deep Sea Res., Part I*, *42*, 641–673.

Rintoul, S. R., and S. Sokolov (2001), Baroclinic transport variability of the Antarctic Circumpolar Current south of Australia (WOCE repeat section SR3), *J. Geophys. Res.*, *106*, 2815–2832.

Rintoul, S. R., C. W Hughes, and D. Olbers (2001), The Antarctic Circumpolar Current system, in *Ocean Circulation and Climate*, edited by G. Siedler, J. Church, and J. Gould, pp. 271–302, Academic, San Diego, Calif.

Sabine, C. L., et al. (2004), The oceanic sink for anthropogenic CO_2, *Science*, *305*, 367–371.

Sallée, J.-B., K. Speer, and R. Morrow (2008), Response of the Antarctic Circumpolar Current to atmospheric variability, *J. Clim.*, *21*, 3020–3039.

Sallée, J.-B., K. Speer, and S. Rintoul (2010a), Zonally asymmetric response of the Southern Ocean mixed-layer depth to the Southern Annular Mode, *Nat. Geosci.*, *3*, 273–279.

Sallée, J.-B., K. Speer, S. Rintoul, and S. Wijffels (2010b), Southern Ocean thermocline ventilation, *J. Phys. Oceanogr.*, *40*, 50–529.

Sarmiento, J. L., N. Gruber, M. A. Brzezinski, and J. P. Dunne (2004), High-latitude controls of thermocline nutrients and low latitude biological productivity, *Nature*, *427*, 56–60.

Sen Gupta, A., A. Santoso, A. S. Taschetto, C. C. Ummenhofer, J. Trevena, and M. H. England (2009), Projected changes to the Southern Hemisphere ocean and sea ice in the IPCC AR4 climate models, *J. Clim*, *22*, 3047–3078.

Simmons, H. L., S. R. Jayne, L. C. St. Laurent, and A. J. Weaver (2004), Tidally driven mixing in a numerical model of the ocean general circulation, *Ocean Modell.*, *6*, 245–263.

Sokolov, S., and S. R. Rintoul (2002), Structure of Southern Ocean fronts at 140°E, *J. Mar. Syst.*, *37*, 151–184.

Sokolov, S., and S. R. Rintoul (2007), Multiple jets of the Antarctic Circumpolar Current south of Australia, *J. Phys. Oceanogr.*, *37*, 1394–1412.

Sokolov, S., and S. R. Rintoul (2009), Circumpolar structure and distribution of the Antarctic Circumpolar Current fronts: 2. Variability and relationship to sea surface height, *J. Geophys. Res.*, *114*, C11019, doi:10.1029/2008JC005248.

A. S. Budnick, S. M. Downes, and J. L. Sarmiento, Program in Atmospheric and Oceanic Sciences, Princeton University, 300 Forrestal Rd., Princeton, NJ 08544, USA. (abudnick@princeton.edu; sdownes@princeton.edu; jls@princeton.edu)

R. Farneti, Earth System Physics Section, ICTP, Strada Costiera 11, I-34151 Trieste, Italy. (rfarneti@ictp.it)